

*Department of physics, École Normale Supérieure, Paris
Swiss Plasma Center, EPFL, Lausanne*

TRAPPED ELECTRON MODE
CHARACTERIZATION BY SHORT PULSE REFLECTOMETRY

Master Thesis 2024

Andrea Combette



Supervisors:

Dr. Oleg Krutkin

Pr. Jean François Allemand



Contents

<p>1 Theoretical Background 2</p> <p>I Nuclear Fusion 2</p> <p> 1 Fusion Reaction 2</p> <p> 2 Tokamak confinement 2</p> <p>II Transports in Tokamak 3</p> <p> 1 Trapped particles and drifts 3</p> <p> a) Trapped particles 3</p> <p> b) Drift waves 3</p> <p> 2 Radial Transport 4</p> <p>III Wave propagation in plasma 4</p> <p> 1 Plasma as a medium 4</p> <p> 2 Wave equation 5</p> <p>IV CUWA code overiview 5</p> <p>2 Linear Regime Study 6</p> <p>I 1 dimensional study 6</p>	<p>1 Perturbed Density Profile 6</p> <p>a) General perturbation profile 6</p> <p>b) Step-like perturbation 6</p> <p> b).1 Model 6</p> <p> b).2 Results 7</p> <p>3 1 dimensinal Model 8</p> <p>I Reliable metrics 8</p> <p>II Machine Learning Model 8</p> <p> 1 structure 8</p> <p>III Input Data 9</p> <p>IV Results 9</p> <p>4 2 dimensinal Model 10</p> <p>1 Pulse shape Study 10</p> <p>2 Gaussian fitting of the pulse 11</p> <p>I Model collapses 11</p> <p>II 1 dimensional study 11</p>
---	--

ABSTRACT

ONE of the common goals in experimental magnetically confined fusion research is characterization of the plasma turbulence. To that end, TCV tokamak features a novel short-pulse reflectometry (SPR) diagnostic, which can potentially be utilized to measure properties of the turbulence. It is essentially a radar system, where the plasma is probed by a short (under ns) microwave pulse in the presence of the cut-off (reflection) area from which the pulse reflects back into the probing antenna. The position of the cut-off for a particular probing frequency (50-75 GHz) range is determined by the plasma electron density. Thus, by measuring the delay between probing and reflected pulse corresponding to different probing frequencies, the information about the electron density profile is inferred including its turbulent perturbations. Unfortunately, the complex interaction of microwaves with magnetized plasma makes it difficult to establish the connection between SPR measurements and properties of the turbulence. Numerical modeling utilizing the synthetic diagnostic approach was carried out to establish this connection for the case of low turbulence amplitudes (linear regime). However, the case of large turbulence amplitudes (nonlinear regime) is yet to be explored. Within the project a systematic analysis of the SPR diagnostic in the nonlinear regime will be carried out. The numerical finite difference code CUWA, which solves the wave equation for a given plasma density, magnetic field and provides synthetic reflected pulse will be utilized. The main goal of the project is identifying markers that can be used to determine if the diagnostic is operating in the nonlinear regime and assessing the possibility of determining the turbulence parameters regardless.

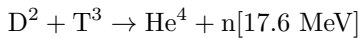
CHAPTER 1

Theoretical Background

I Nuclear Fusion

1 Fusion Reaction

THE nuclear fusion reaction is the process by which two atomic nuclei combine to form a heavier nucleus. It is accompanied by the release or absorption of energy depending on the masses of the nuclei involved. Indeed, the lighter are nuclei, the more energy is released due to the overcoming short-range nuclear force for light nuclei. However, to overcome the Coulomb barrier the reactant must be sufficiently close for a long enough time to allow the quantum tunnel effect between both particles. To do so, we must heat up the reactant to huge temperatures such that these latter are ionizing and turning into plasma. We found that the probability of collision (cross section) is the best for the Deuterium-Tritium mix.



2 Tokamak confinement

The key component of the fusion process is how long we can confine the plasma. This confinement can be of several kinds. One of the most promising and old, is the Tokamak vessel, which uses magnetic confinement to keep the plasma in a toroidal shape. The plasma is heated up to several million degrees, and the fusion reaction can be sustained. The energy released by the fusion reaction is used to heat up the plasma, and to sustain the reaction. The energy balance is given by the Lawson criterion, which is a measure of the energy confinement time over the energy loss time. The energy confinement time is given by the plasma density, temperature and the energy loss time is given by the plasma losses.

$$n\tau E \geq 1.5 \cdot 10^{20} \frac{\text{s}}{\text{m}^3}$$

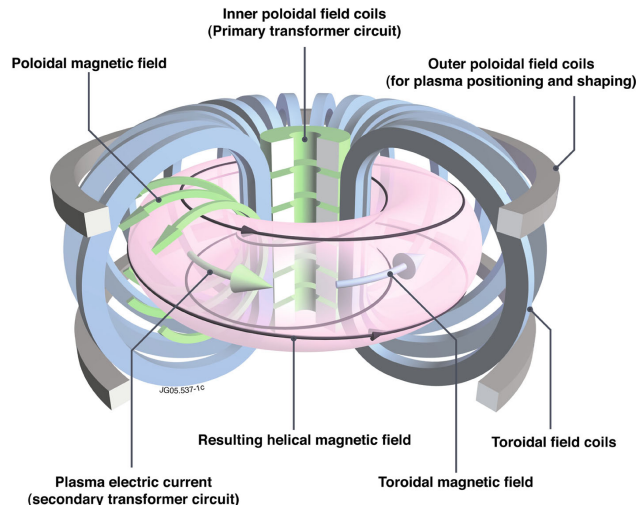


Figure 1.1: simplification of Tokamak device, the toroidal magnetic field is generated by the coils, and the poloidal magnetic field is generated by the plasma current and the poloidal field coils. The plasma is heated up by several device, and the fusion reaction can be sustained.

This confinement is realized by applying a strong magnetic field in the toroidal direction. The magnetic field is generated by a set of coils, which are arranged in a toroidal shape, and the plasma is heated by various method [1]. The neoclassical geometries at stake in the tokamak leads to several physics phenomena such as charge separation in the tokamak, drifts cinematic and turbulences. The curvature and the gradient of magnetic field [2] imposed by the geometry leads to $E \times B$ drift. Which impose to the tokamak a poloidal magnetic field component to counter this effect. This twist in the field line is called the safety factor and is defined as :

$$q(\Psi) = \frac{1}{2\pi} \frac{\delta\chi(\Psi)}{\delta\Psi} \approx \frac{B_{tor}r}{B_{pol}R},$$

With χ the toroidal magnetic flux. This safety factor is one of the most important measures in tokamak since the induced magnetic properties on the rational magnetic surface ¹ are of paramount importance for the confinement of the plasma. Indeed, we can define the shear stress as $\hat{s} = \frac{r}{q} \frac{dq}{dr}$, which measures how much the magnetic field line are twisted along the small radius of the tokamak. This shear explains why the turbulences grow on rational surfaces (no Landau Damping

¹Only rational value of the safety factor allows periodic field line



$k \cdot B = 0$, [3]), and how they are damped into bigger scale flow (zonal flow) see [4]. Indeed, the consideration of the magnetic surfaces is also at the foreground for solving Ballooning equations in toroidal geometry, since it will drive the definition of the toroidal functions of Ballooning modes, every discussed instabilities can be expressed using a toroidal geometry in the Ballooning space [5, 6]. In addition to that the safety factor allows to have an insight of the strength of the toroidal current, which follows the q -profile (max in the center), this explains why the toroidal velocity of particle is lower on the edge than in the center, which allows some particle to be trapped in banana orbits.

II Transports in Tokamak

Anomalous transport is a crucial subject in tokamak research, indeed it causes a huge drop of the energy confinement through enhanced particle radial flux. Here we will study micro-instabilities, i.e small scale turbulences (gyro-bohm scaling [4]), whose radial transport is really high and largely controlled by low frequency modes [6]. For these type of instabilities, the study is based on Kinetic Vlasov theory. Several types of micro-instabilities exists from **TEM** to **ITG** and **ETG** instabilities. These instabilities cause a transport of energy from the core of the plasma to the edge, where it can be evacuated, the largest transport in the TCV is due to the unstable **TEM** mode [7, 8]. This mode is the results of the resonant interaction between trapped electron and Drift Wave (DW), it can be collisionless or dissipative, basically the trapped electron are transferring energy to the growing wave.

1 Trapped particles and drifts

There are two type of kinetic for electrons in the tokamak : run-away or passing and trapped electrons. Majority of the electrons are passing since to be trapped electrons must verify : $v_{\parallel} \ll v_{th}$ [9][10]. However trapped electrons present a transit time much larger than passing one, this leads to greater interaction with the DW. These different of behavior regarding the DW leads to small scale instabilities.

a) Trapped particles

For a collisionless plasma $\nu \ll w$, with ν the collision frequency and w the frequency of the considered wave, the main radial transport is caused by particle with low parallel velocity. Indeed, when the toroidal component of the magnetic field is much larger than the poloidal component, $|B_{\Phi}| \gg |B_{pol}|$ we have the simple B relation for a torus

$$B \propto \frac{1}{R - R_0},$$

then in the (r, θ, z) coordinates we have :

$$B = B_0 \left[1 - \frac{r}{R_0} \cos(\theta) \right]$$

Hence, taking into account the toroidal drift we can derive the following equations using the guiding center equations [9]:

$$\frac{d}{dt} \left(r + \frac{m}{qB_p} v_{\parallel} \right) = 0, \quad r - r_0 = -\frac{m}{qB_p} v_{\parallel}$$

r_0 indicates the position of the turning point where the mirror effect occurs [11]. To be trapped the particle velocity should verify $v_{\parallel} \ll v_{\perp}$ more precisely from a simple energetic approach [8]

$$0 \leq v_{\parallel} \leq \sqrt{2\epsilon}v_{\perp}.$$

This partially explains why the velocity distribution of the electron [8, 10] is modified from a Boltzmann distribution to a more complex one, leading in a drop of conductivity (Spitzer conductivity). This also explain why the **TEM** dissipative and collisionless are highly localized in the trapped electron region. The banana shape formed has then the following width :

$$\Delta r = \frac{m}{qB_p} v_{\parallel}$$

This banana shape can be interpreted as a simple Lorentz force acting on the particle animated by a sufficiently high vertical drift motion.

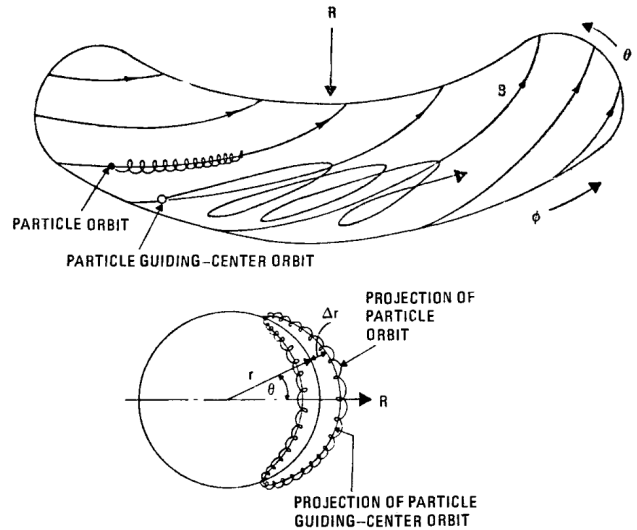


Figure 1.2: Trapped particle motion in the tokamak, the banana shape is due to the toroidal magnetic field, the particle is trapped in the magnetic well, and can interact with the DW. the second figure shows a cross section of the torus where we project the one banana orbit of the particle. From [9, 10]. Hence, if a wave is resonating with the particle, with a lower frequency than the transit time of the particle, the particle can exchange energy with the wave in a quasi-adiabatic way. (see after)

b) Drift waves

Electron DW instabilities that are at stakes here are governed by the famous **Hasegawa-Wakatani** [12, 13] equation due to non-adiabatic response of the electrons (the equilibrium is not reached after each oscillation of the wave) derived from a simple version of the drift kinetic equation from Vlasov theory. Hence, let's remind the general form of the general form of the H-W equation :

$$\begin{cases} \rho_s^2 \frac{d}{dt} \nabla_{\perp}^2 \Phi = D_{\parallel} \nabla_{\parallel}^2 (\tilde{\Phi} - \frac{T\tilde{n}}{|e|n_0}) \\ \frac{1}{n_0} \frac{d}{dt} \tilde{n} + \frac{v_r}{n_0} \partial_r n_0 = D_{\parallel} \nabla_{\parallel}^2 (\tilde{\Phi} - \frac{T\tilde{n}}{|e|n_0}) \end{cases} \quad . \quad (1.1)$$



With ρ_s the ion sound radius, D_{\parallel}^2 the parallel diffusion coefficient, Φ the electrostatic potential, \tilde{n} the density perturbation, v_r the radial velocity, n_0 the equilibrium density, T the electronic temperature, e the electron charge.

In the adiabatic limit [14], i.e when the particles diffuse faster than the wave, we can assume a simple a Boltzmann distribution of electrons with a small perturbation :

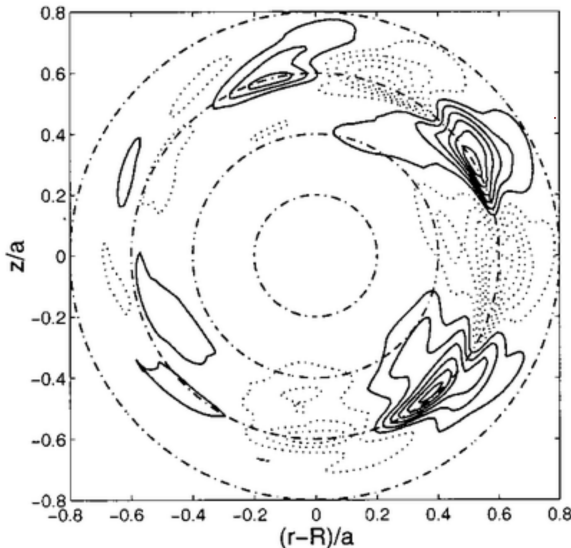
$$\frac{\tilde{n}}{n} \approx \frac{|e|}{T} \tilde{\Phi} + \tilde{h}$$

this finally leads to the **Hasegawa-Mima** [15] equation under the assumption : $v_{thi} < \frac{w}{k_{\parallel}} \ll v_{the}$.

$$\begin{cases} \rho_s^2 \frac{d}{dt} \nabla_{\perp}^2 \tilde{\Phi} \approx \frac{1}{n_0} \left(\frac{d\tilde{n}}{dt} + v_r \partial_r \tilde{n}_0 \right) \\ \partial_t \frac{|e|\tilde{\Phi}}{T} + \partial_r \tilde{h} - \rho_s^2 \frac{d}{dt} \nabla_{\perp}^2 \tilde{P} \tilde{h} + v^* \partial_y \frac{|e|\tilde{\Phi}}{T} = 0 \end{cases} \quad (1.2)$$

With $v_* = \rho_s c_s / L_n$ and L_n the gradient scale of the equilibrium density $-\partial_r n_0 / n_0$. This leads to the following dispersion relation for the drift waves with w_r the real frequency of the wave and γ the growth rate (the imaginary part of the frequency) :

$$\omega_r = \frac{w_*}{1 + k_{\perp}^2 \rho_s^2}, \quad \frac{\gamma}{w_r} = \pi \frac{w_r - w_*}{k_{\parallel} v_{e,th}}$$



We can denote $\frac{w-w_*}{k_{\perp}^2 v_{e,th}}$ the non-Boltzmann factor for electron DW. The reader will note that this study is independant of trapped electron, this is why in order of magnitude the growth rate is quite low, however when we increase the transit time of electron (by trapping), we can show [Sazn_diego], that the non-Boltzmann factor is increasing, leading to a higher growth rate, notably because of the introduction of $w_{D,e}$ the electron curvature drift frequency. Indeed, for colisionless trapped electron mode the non-Boltzmann factor is given by : $\frac{w-w_*}{w_{e,D}} e^{-R/L_n} \sqrt{\frac{R}{L_n}}$ which is definitively larger than the electron DW non-Boltzmann correction factor. leading to the following growth rate :

$$\frac{\gamma}{w_r} = i\pi \frac{w-w_*}{w_{e,D}} e^{-R/L_n} \sqrt{\frac{R}{L_n}},$$

explaining why **CTEM** are much more unstable than classical electron DW. Explaining also why the main instabilities are located in the banana region where the coherence time of the electrons are much more larger, same conclusions can be driven from the Dissipative Trapped electron mode [14]. This instabilities leads to inverse cascade of energy (*Kolmogorov*), contributing to highly non linear interaction with mesoscale structures (zonal flow) [6, 7, 16].

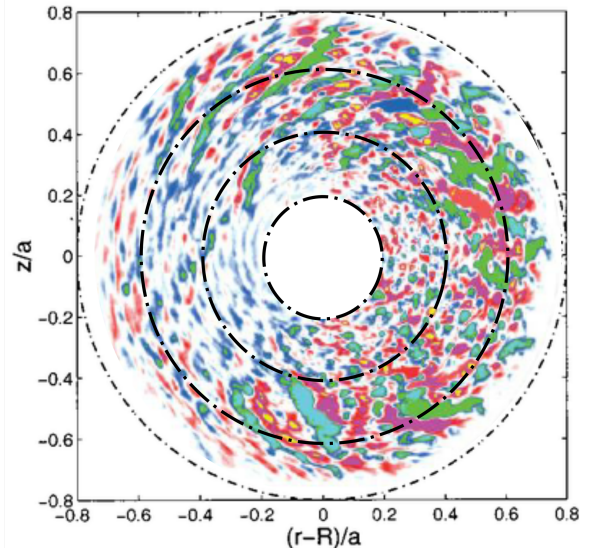


Figure 1.3: Cross section view of tokamak with negative shear flow - On the left we have the fourier Ballooning mode $n = 6$, characteristic from the TEM mode, it presents this characteristic tilting of the wave vector k_{\perp} , and a radial translational symmetry. On the right we have a simulated TEM mode, with the same shape structure characteristics, we will note the presence of multiple modes, teared and more tilted by the zonal flow, explained by the non linear interaction between these two types of flow, reproduced from [17, 18]

2 Radial Transport

part.

These micro-instabilities are one of the best candidates to explain high radial transport, indeed as we saw previously the resonating trapped electron allows a high fluctuation in the density field and in the magnetic pressure. Indeed we can show that the radial particle flow does not vanishe (as normal), in this case with a high contributio of the resonant trapped electron to the mean transport [16]. This radial dependency is the only density dependency retained for the following

III Wave propagation in plasma

1 Plasma as a medium

To study the density profile, many diagnostics methods exists ,like Doppler Reflectometry, RCDR, Short

²the parallel diffusion coefficient provides insights of the electrons-ions collision frequency $D_{\parallel} = \frac{v_{the}^2}{\nu_{ei}}$



pulse reflectometry ... The study here will be based on the Short Pulse Reflectometry (**SPR**), this method consists in probing the magnetized plasma with short Pulse (<ns) microwaves operating in the time domain at a fixed frequency under normal incidence with respect to the cut-off surface and the variation of the delay of the reflected pulses. The probing signal, is sensitive to density variation since it will change the cut-off position, this is why it can be used to have deeper insights of the turbulences characteristics

2 Wave equation

Assuming a monochromatic electromagnetic-wave and using the Maxwell equations, we can derive the local complex dielectric tensor, and the considered wave wave equation :

$$\nabla^2 E - \vec{\nabla} \nabla \cdot E = -\frac{\omega^2}{c^2} \hat{\epsilon} E \quad \left. \begin{array}{l} \hat{\epsilon}_{ik} = \delta_{ik} - \frac{4\pi i}{\omega} \sigma_{ik} \end{array} \right\} \quad (1.3)$$

with σ_{ik} the conductivity tensor. To establish this equation multiple assumption have been made, linear Ohm's law is applicable, cold plasma (cite), neglect chaotic motion of the particles, which implies neglecting the kinetic effect. To simplify the problem we will assume the plasma to be stationnary and neglect all kinds of damping. Then in a carthesian coordinates system with z axis driven by a constant magnetic field, $\vec{B} = B_0 \vec{e}_z$, we can derive the following dielectric tensor[Thomas H.Stix]

$$\hat{\epsilon} = \begin{pmatrix} \epsilon & ig & 0 \\ -ig & \epsilon & 0 \\ 0 & 0 & \eta \end{pmatrix}$$

$$\text{With : } \epsilon = 1 - \frac{\omega_{pe}^2}{\omega^2 - w_{ce}^2}, g = \frac{w_{ce} w_{pe}^2}{w(w^2 9 W_{ce}^2)} - \frac{w_{ci} w_{pi}^2}{w(w^2 9 W_{ci}^2)}; \\ \eta = 1 - \frac{w_{pe}^2}{w^2} - \frac{w_{pi}^2}{w^2}; \quad w_{pi} = \sqrt{\frac{4\pi n e^2}{m_i}}; \quad w_{ci} = \frac{eH}{m_i c}$$

w_{pi} stands for the electron or plasma frequency and w_{ci} is the cyclotron frequency for the i species. We will consider the electron component preponderant in the next study since we are dealing with microwave frequency. The wave equation can be simplified to the following :

$$\left. \begin{array}{l} (S_{yz} - \epsilon)E_x - igE_y - \Pi_{xy}E_z = 0 \\ (S_{zx} - \epsilon)E_x + igE_x - \Pi_{yz}E_z = 0 \\ (S_{xy} - \eta)E_z - \Pi_{xz}E_x - \Pi_{yz}E_y = 0 \end{array} \right\} \quad (1.4)$$

Defining : $S_{ij} = N_i^2 + N_j^2$; $\Pi_{ij} = N_i N_j$; $N_i = \frac{k_i w}{c}$
For the **SPR** study the wave is perpendicular to the external magnetic field, hence we can simplify the system to the following :

$$\left. \begin{array}{l} (N_y^2 - \epsilon)E_x - igE_y = 0 \\ (N_x^2 - \epsilon)E_y + igE_x = 0 \\ (S_{xy} - \eta)E_z = 0 \end{array} \right\} \quad (1.5)$$

Which leads to two different types of solution respectively the ordinary mode (\mathcal{O}) and the extraordinary mode (\mathcal{X}).

\mathcal{O}	\mathcal{X}
$S_{xy} - \eta = 0$	$(N_y^2 - \epsilon)E_x - igE_y = 0$
$E_y = 0$	$(N_x^2 - \epsilon)E_y + igE_x = 0$
$E_x = 0$	$E_z = 0$

The \mathcal{O} mode corresponds to the mode with electric field parallel to the external magnetic field, hence the propagation does not depend on this latter but only on the density profile. The \mathcal{X} mode is the mThisode with electric field perpendicular to the external magnetic field, hence the propagation depends on the magnetic field and the density profile. The dispersion relation of the wave can be derived locally from the wave equation, and we can obtain :

$$k^2 = \frac{w^2}{c^2} \eta \approx \frac{w^2}{c^2} \left(1 - \frac{n}{n_c} \right); \quad n_c = \frac{m_e w}{4\pi e^2} \quad (1.6)$$

Here we can see that the wave number vanish at $n = n_c$, this is the cut-off layer where the wave is reflected. The k-spectrum of the \mathcal{X} is much more complicated and include plasma resonances where thermal effects must be taken into account. For this study we will limit ourself to the \mathcal{O} mode. Then from solving the Helmotz equation (local dependancy of the wave number)

$$\frac{\partial^2 E_z}{\partial x^2} + k(x)E_z = 0$$

and appying the **WKB** approximation (slow variation of the plasma parameters), i.e assuming a a solution of the form $E_z = A(x) \exp(i\Phi(x))$, with A varying slowly and Φ varying quickly, we can derive the following expression for the Electric field:

$$E_z(x) = \frac{E_z}{\sqrt{\frac{c}{w} k(x)}} \exp \left(i \int_0^x k(x') dx' \right)$$

The WKB approximation will be used in the one dimensional approach (see Chapter 2), and in the **CUWA** code for computing the ray tracing in order to adjust the size of computation Yee cells [19] and the computation domain.

IV CUWA code overiview

The CUWA code is a **GPU** based computations scheme with a Python-CUDA frameworks, using finite difference scheme for spatical dependancy applied to the three different fields : E, B, J and the well-known leap-frog time stepping. It is used to simulate the propagation of electromagnetic wave inside a "cold plasma". The sqaial finite difference scheme is based on the FDTD Yee's method [**Yee**], with slight modifications. It solves the discrete version of the Maxwell's equations with a cold Plasma current Response \mathbf{J} :

$$\left. \begin{array}{l} \frac{\partial}{\partial t} \mathbf{B} = -\nabla \times \mathbf{E} \\ \frac{\partial}{\partial t} \mathbf{E} = c^2 \nabla \times \mathbf{B} - \frac{\mathbf{J}}{\epsilon_0} \\ \frac{d}{dt} \mathbf{J} \nu \mathbf{J} = \epsilon_0 w_p^2 \mathbf{E} - \mathbf{J} \times \mathbf{w}_c \end{array} \right\} \quad (1.7)$$

with w_p the electron plasma frequency, ν the electro collision frequency and w_c the electron cyclotron frequency. To limit the computational cost, the computation domain is amended with a convolutional perfectly matched layer (**PML**) to ensuring any reflected singals are small (well used in open boundaries system). It can be viwed as a sponge layer for electromagnetic wave.

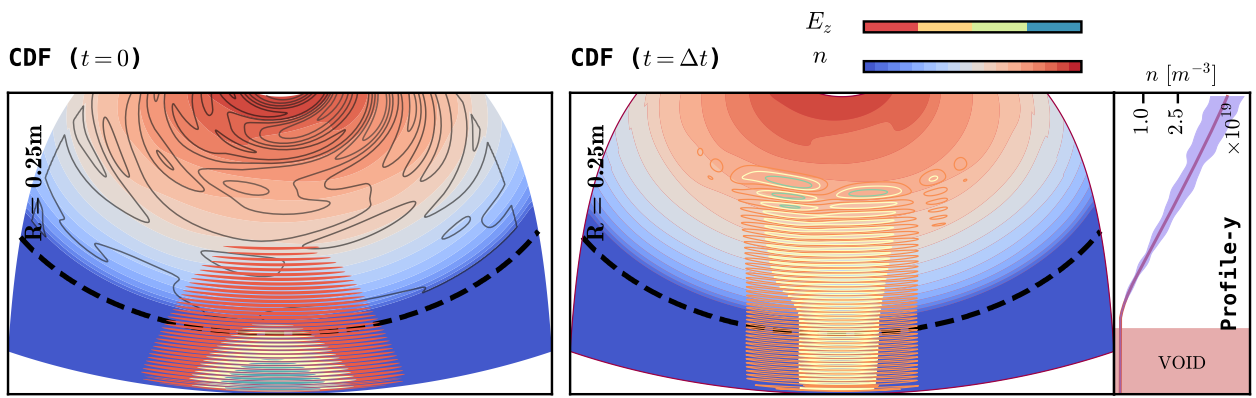


Figure 1.4: SPR setup using the *O.Krutkin and A.combette LEONARDO* simulations from the **CUWA** code, the probing wave is sent to the plasma, and the reflected wave from the cut-off is measured, the delay between the two waves is a measure of the plasma density profile, in addition to the pulse shape that has been altered by the turbulences (eq). Here we plot the contours of the density profile, with cold density perturbations (black contour lines on the left plot), the probing wave is reflected by the cut-off layer (initial probing wave on the left and after a $\Delta t \approx 10\text{ns}$ we got the reflected scattered wave on the right). The third plot on the right shows the density profile width its perturbations (filled), a liner density profile

$$n(x, y) = \frac{x}{L} (n_c + \delta n(x, y)).$$

as been chosen according to (cite). Note that this linear correction made on the amplitude of the turbulence fields, follows from the non-adiabatic perturbations [16], and his more relevant than a simple constant amplitude turbulence field. The curvature of the grid has been set to the $R = 0.25\text{m}$ to mimic the TCV geometry.

CHAPTER 2

Linear Regime Study

The goal of this study is to find a way to link the plasma density perturbations to the reflected pulse characteristics. First we will study a simple 1 dimensional model proposed by (*Oleg Krutkin*) applied in a given range of turbulence amplitude and size and then we will extend this study to a more general 2D model using the **CUWA** code.

I 1 dimensional study

Assuming a simple plasma density profile $n(x)$, we can study the wave propagation in the plasma. The goal of this approach is to find a way to link the plasma density perturbations to the reflected pulse delay. To retrieve some information about the pulse delay we will use a statistical approach to get rid of the randomness implied by the perturbations considerations. The delay of the probing wave is given by the following formula :

$$\tau_c = 2 \int_0^L \frac{dx}{v_g}$$

Where v_g is the group velocity of the wave, L is the position of the cut-off. From the simple assumption $\langle \delta n \rangle = 0$ for an Ordinary mode the v_g expression obtained [] can be used to expand the integral to the following :

$$\frac{2}{c} \int_0^L \frac{dx}{\sqrt{1 - \frac{x}{L} - \frac{\delta n}{n_c}}}$$

The main contribution of this integral comes from the vicinity of the cut-off layer, Where the group velocity is the smallest. We can discuss the relevance of

this expansion this the main contribution of the integral comes from the cut-off region where the WKB approximation cannot be applied.

1 Perturbed Density Profile

a) General perturbation profile

First let's consider to simplify a gaussian perturbation density profile (we will see later that the spectrum of the vector number is not a gaussian but a non trivial power spectrum due to the two type of energy cascade). From this, the considered integral can be written in the following way :

$$\tau_d = \frac{2}{c} \int_0^L \frac{dx}{\sqrt{1 - \frac{x}{L} - \frac{a \exp\left(-\frac{(x-L)^2}{8l_{cx}^2}\right)}{n_c}}}$$

This integral is not trivial to solve in from an analytical way, which is necessary to exhibit the possible statistical features of the dealay. This is why we can suggest developing a first order perturbation profile which leads to step like perturbations.

b) Step-like perturbation

b).1 Model With a step-size perturbation characterized by l_{cx} length. This allows to get an analytical expression of the integral for different density profile. However, to get this simplification, we need to assume that the perturbation is small enough such that the WKB approximation can be applied. This is the case for the linear regime, where the perturbation is small enough such that the cut-off layer is not too much perturbed (i.e $\delta_x \ll l_{cx}$). In the case of a large perturbation, an other step perturbation localized far from the cut-off layer can be used to get the same result,



which breaks the main assumption of this approach (see fig.1). It's relatively trivial to obtain the following expression for the delay [cite Krutkin] :

$$\tau_d = \frac{4L}{c} - \frac{2L}{c} \sqrt{\frac{L}{l_{cx}} \frac{\delta n}{n_c}}$$

The statistical approach is to consider the perturbation as a random variable, and to compute the statistical properties of delay of the probing wave. This approach is relevant for the linear regime, where the perturbation is small enough such that the cut-off layer is not too much perturbed (i.e $\delta_x \ll l_{cx}$). For example

we can compute the standard deviation of the delay depending on the standard deviation of perturbations. This gives us the following at first order :

$$\sigma_{\tau_d} \approx \frac{2L}{c} \sqrt{\frac{L}{l_{cx}} \frac{\sigma_{\delta n}}{n_c}}$$

To test this assumption we can compare the analytical expression with the numerical integration of the wave equation, for numerous gaussian perturbations with characteristics length l_{cx} and various amplitudes δn , depicted in the figure 2.2.

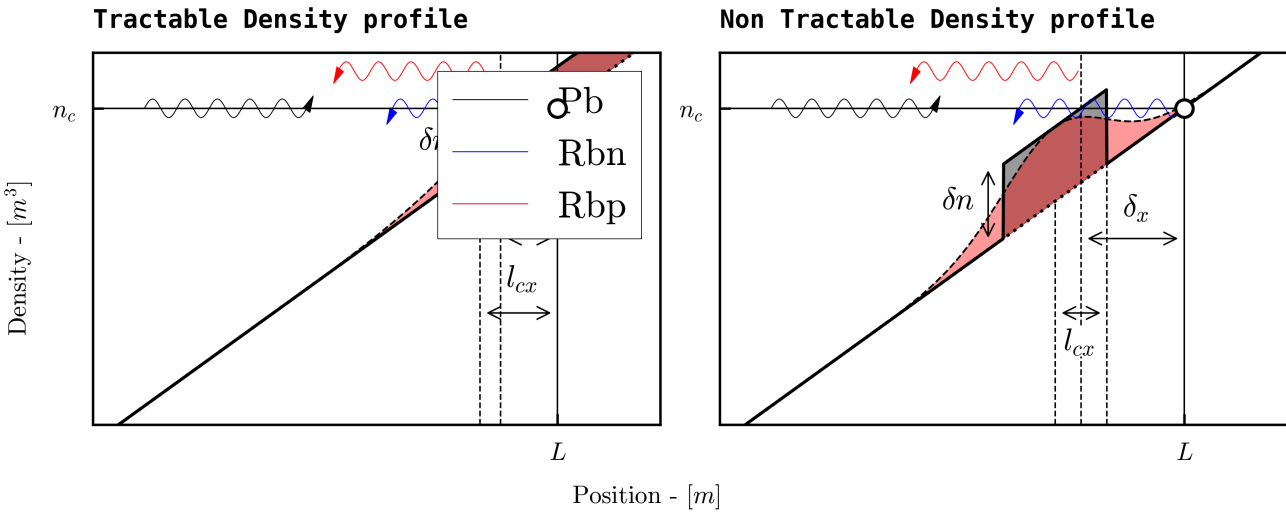


Figure 2.1: Here we plot the density profile of the plasma for different perturbation amplitude, in grey the step-like model perturbation and in coral the gaussian one. For large value density perturbation, the model leads to a contradiction with its assumption $\delta x < l_{cx}$ or $\delta n < n_c \frac{l_{cx}}{L}$, given by a small cut-off layer shift. The blue Pb wave is the probing wave, red Rbp wave is the reflected one and blue Rbn wave is the normal reflected wave, in absence of perturbation.

One sample of density fluctuation is produced using the following formula, to match a supposed gaussian spectra of instabilities :

$$\delta n(k_x) = \delta n_0 \exp \left(-\frac{(kl_{cx})^2}{8} + i\Phi(k) \right)$$

with $\Phi(k)$ a random phase, k the radial wavenumber of the density perturbation and δn_0 the amplitude of the perturbation, this amplitude can be taken constant or dependant of the radial position according to the kind of profile we use. Then we inverse fourier transform this density perturbation to get the density profile in the real space. Finally, for each sample, the delay is then numerically integrated from the formula [cite delay], using simple trapezoidal integration.

numerically integrated delay, which stands as reference is in black cross. The second order analytical formula presents a characteristic drop-off (as the simulated delay) after reaching a critical value amplitude. This critical value can be defined by two ways [PUT, 20] and fix the threshold of what we could later the **Non linear regime**. Which can suggest than expanding further the σ_{τ_d} which leads to a better handling of non-linear domain. However, in both cases some discrepancies are observed for large perturbations in Non Linear regime, but the analytical expression seems to be a good approximation for small perturbations, except for really tiny one [cite]. However, one have to introduce a correction factor to the analytical expression to get a better agreement with the numerical integration. This l_{cx} dependant factor is given has not been studied yet but it highlights the limitations of current step driven 1D model ¹. The non linear regime is strongly related to scattering effect, which are not taken into account in this approach. In addition to that, generally the density corrugation reaches a level of 100 % of the density value near the cut-off [7], especially since the adiabatic and non adiabatic component of the electron response have the same potential dependency [16]. Hence the non-linear regime is non negligible and of necessity to find a sufficiently precise model to evaluate turbulences amplitudes in **NL** regime.

b).2 Results The results are shown in the figure 2.2, the simulated deviation of delay (black cross) was computed on 10000 samples to ensure statistical stability, with a 50 GHz probing wave and a $2L$ integration domain, allowing us to take into account negative perturbation near the cut-off, indeed if there are multiples ones near the standard cut-off it might strongly shift this latter. The plain black line is the 1st order approximation of the formula [eq] and the dashed one as the third order approximation of the second formula. The

¹The integration of the gaussian integral was also tackled, with a second order bell-approximation, leading to logarithmic dependancies over the plasma parameters, however the formula was too complicated to exhibits the statistical properties of the delay refers to appendix

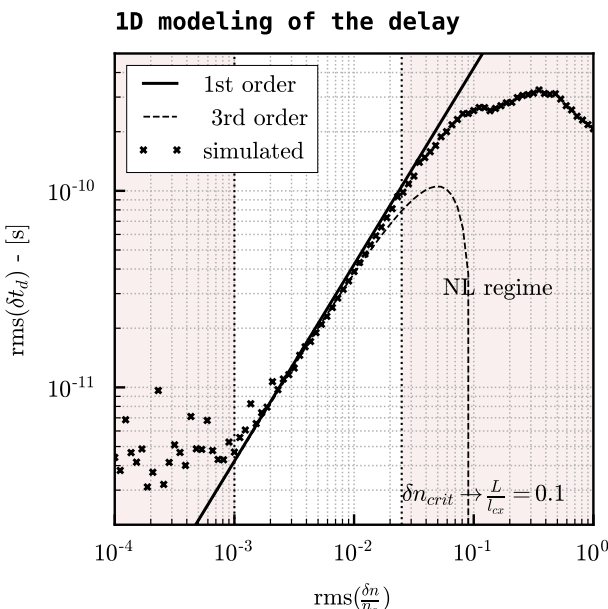


Figure 2.2: 1 dimensional predicted amplitude of the analytical 1st and 2nd order step driven model, compared to the simulated 1 dimensional delay see eq :1.6, a constant δn_0 has been used for the density profile

Hence, the first arised issue is to find a good parametrization of the model (i.e find the best statiscial metrics) to predict the amplitude of the turbulence. This study will be done using several profile of density perturbations amplitudes δn_0 , to see if the model we build is sufficiently robust to adapt.

CHAPTER 3

1 dimensinal Model

The first model we tried to build relies simply on the 1 dimensional integration of the delay. Hence, for this simple model wa can only rely on the pulse delay statistical properties. Several options had been tested from the study of the quantile repartition of the delay, its histogram , and several statiscial properties of this latter. Then the study consists in a simple multidimensional regression problems where we will try to estimate the amplitude of the perturbation and the non-perturbed delay of the probing wave (i.e without the turbulencs fields) and this for several density profile. In order to tackle this problem we used a stacked regressor, combined with a multi-output one.

I Reliable metrics

To train our Machine Learning model, we need some clear data, with the best input as possible. So first let's try to understand the characteric of the delay. To have a general overview of the influence of the turbulence amplitude δn_0 on the delay characteric, the best way is to study the distribution of this latter in function of the amplitude, this is done in the following plot.

Normalized Delay Violins

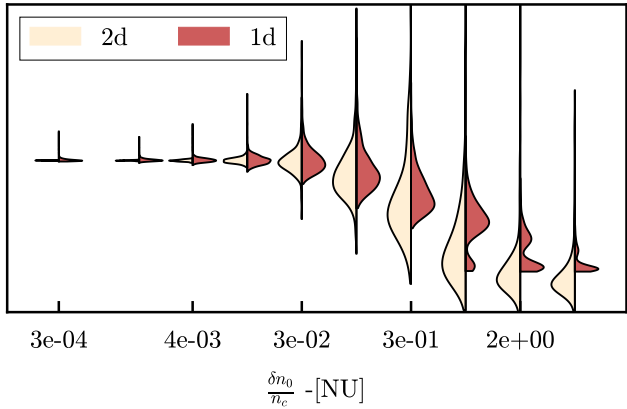


Figure 3.1: Violins plot of the delay distribution over δn_0 , Here we choose for a simple first apporach a simple linear profile with δn_0 independant of the radial position. The left side of each violins stands for the 2d distribution of the delay for comparison.

The first thing that we can unearth is that the delay distribution is well disturbed by an amplitude increasing, the mean delay decrease (which is quite obvious see ??), the standard deviation of the delay increases and when we reached the non-linear regime it starts decreasing. The distribution seems also to be more more skewed until we reach the non linear regime, this indicates that the study of the momemt of the delay distribution can also be a good way to predict the amplitude level. The two-simulation sets present quite the same behaviour, however at high amplitude the 1d simulation set present some discrepancies with the 2d one, indeed the distribution is more eratic, this can question the good convergence of the 1D integration (see : 1.6). Still, the delay study should lead to a good estimation for both simulation sets, even without pulse shapes study allow with the 2D model. Hence, let's see if the delay study can be a sufficient estimator for amplitude level prediction in both dimensionalities.

II Machine Learning Model

The machine Learning model will learn to predict the amplitude δn_0 and the default delay without amplitude τ_0 , with one one dimensional training set, and will be test on a one dimensional and a two dimensional testing set.

1 structure

The regression model we used is a stacked-multioutput regressor, it combines the following models : K-neighbors (KNN), Random-forest (RF), 3 different Gradient-Boosting (GB, LGBM, XGB), and support vector (SVR) , regressors, it is made to be as general and versatile as possible. Then the 6 models are trained in parallel on the same training datasets, in series with a decision regression model which is in our case a final RF layer trained on the outputs of previous layers.T Normally the Gradient-Boosting models can not handle multi-output regression, this is why we used a multi-output RegressorChain. This model train the model to predict the the first entry and then to predict the second given the first prediction, this allows to incorporate a dependancy between the different outputs, which should not be the case here, so normally a simple MultiOutputRegressor should be sufficient. Let's

note that the score of the final model cannot be less than the score of the best model. The following table described the hyperparameters used for the stacked model.

Model	Hyperparameters
KNN	n_neighbors : 20
RF	n_estimators : 300 max_depth : 40
GB	n_estimators : 200 lr : 0.005
LGBM	n_estimators : 200 lr : 0.005
XGB	n_estimators : 200 lr : 0.005
SVR	kernel : 'rbf' C : 1 epsilon : 0.01

Table 3.1: Main Hyperparameters used for the stacked model, the error use is not detailed as long as the performance tweaks

III Input Data

For the 1D based trained model, we can only use the delay distribution as input variables. We tried several moment of the distribution as input (mean, variance, skewness...), combined with the discretized delay distribution. We tested two types of discretization, the binned distribution and the quantile distribution. However, we reached better results with the quantile study of the distribution, coupled with the moments as input. This allows the model to have a direct connection between the output τ_0 and the quantilized distribution. We use in both case 30 quantiles to discretized the distribution. The 1D simulations set is then processed, splitted in a training and a testing set (80/20 ratio) and finally standardized, the amplitude parameter was used with its logarithmic value because it was find to be more efficient. Hence we arrived to a final input shape of 33 features and ~ 3000 samples, including the L , l_{cx} paraemters in the input data. For the 1D simulation, we introduced a random shift in the delay distribution for each sample, indeed if we dont do that the model will learn τ_0 value from the highly correlated parameter L (originally L is linear with τ_0) which might be not the case in experimental data, where L can stand for the gradient scale at the cut-off [7]. For this study we used several density profiles to see if they have a real impact on the learning process of the model. For the 1D simulations the dependancy over y is dropped. For the linear background profile, the global density profile will be the following :

$$n(x, y) = n_c \frac{x}{L} + \delta n_0(x) \delta n(x, y).$$

With δn the 2D gaussian turbulence profile For the quadratic background profile L , stands for the gradient scale at the cut-off, and δn_0 the turbulence amplitude profile . Here we choose the following formula to get the value of 1 of the gradient at L , which gives us :

$$n(x, y) = n_c \left[1.25 - \frac{(1.5L_0 - x)^2}{L_0^2} \right] + \delta n_0(x) \delta n(x, y)$$

The dependancy of δn_0 will take severql form, from constant to linear, quadratic or exponentially ponderated [20], this scaling of the turbulences is done to mimic the true turbulence profile (REF), and to avoid the non natural preponderance of turbulences while working with small amplitudes.

IV Results

From this we reach a final score of 0.94 without the moment and 0.96 with the moments on the 1d test datasets. However, with the 2d datasets the results appear to be catastrophics. The model generally predict an amplitude level one odm bellow or higher than the real one. A goos way to evaluate the model is to study the residuals of this latter for each parameters value of the testing set. It allows to have a quick overview of the performance model, and on the impact of parameter value on the model performances.

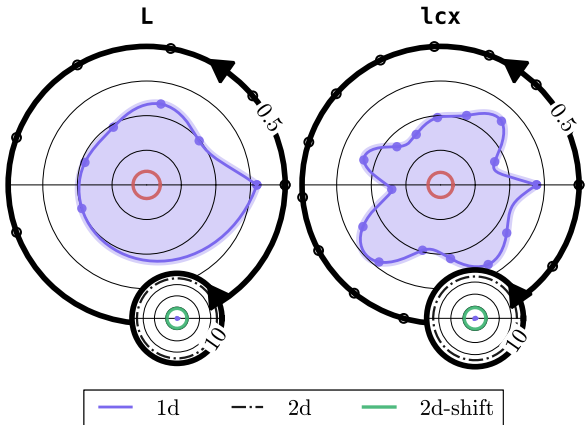


Figure 3.2: Plot of the amplitude residuals of the model for the 1D testing set in Non linear regime, the residuals are meanned given a value of the studied simulation's parameter. The filled curved stands for the amplitude residuals exponentially rescaled to the real amplitude value, The red line in the center of the plot is the τ_0 mean residuals, far bellow the mean amplitude residuals. The second smaller polar shows the comparison of the residuals for several daasetets : the plot of the mean amplitude residuals for the 2D datasets (black dashed curve), the amplitude residuals for the 1D datasets (blue curve in the center), and the plots of the residuals for the 2D datasets shifted to the 1D delay distribution (green curve).

The figure 3.2 unearths quite good results regarding the 1D model prediction for the 1D testing simulation datasets, the predicted is generally of the same order of magnitude than the real one, and the residuals are quite well distributed among all the simulation parameters which is quite comforting. However, when we try to generalize the model to a higher dimension, here 2D simulations we reached very bad results with a mean amplitude residuals value of 10 for any simulations parameters. This can be explained by the fact that 1D simulations does not take into account multiple scattering effect when we reach non linear regime (see 1.6), however we can note that in non-linear regime on the 1D tetsing simulation datasets the model is far more performant than the analytic one. However, one can question the fact that the delay distribution is similar between the 2D case and the 1D case. Indeed, for the



same 1D parameter, we can find a shift between the mean value of the delay for the 2D simulations sets and the 1D simulations set, this is due to the layer of void added around the computation domain in the 2d simulations [20], and also because the pulse is not launched at $t = 0$. Then, if we shift the 2D simulation delay datasets to the 1D simulations delay (which is of course questionable), we reach quite a good score even in non-linear regime (this observation has been done with a flat 2D geometry, and does not take into account crucial 2D simulation parameters as the probing angle or the curved profile), the residuals obtained is the order of 2 times the value of the amplitude which is relatively good knowing the logarithmic scale of the amplitude during the training process.

However, one can ask if the study of the pulse shape with different of its characteristics can lead to better results. Indeed it will allow to take into account the multiple scattering effect, and the dispersive effect of the plasma. This will be the subject of the next chapter.

CHAPTER 4

2 dimensinal Model

1 Pulse shape Study

The pulse shape is also an interesting parameter to study, indeed it can give us some information about the plasma density profile, since the pulse shape can be modified by the presence of perturbations due to multiple scattering effects and dispersive effects [see O mode dispersion relation]. The dependence of the pulse shape over the background density profile will be also studied with linear, quadratic and linear modified perturbation profile.

One can expect to have a much larger and randomness dependent pulse, at high turbulence amplitude due to multiple scattering. Indeed the reflected pulse will be a superposition of all scattered pulse, which should be characterized by a growing tail of the pulse distribution in delay and in width. This can be seen in the figure 4.2. This will be observed on the mean pulse shape, and on the mean statistical parameters of the pulse shape.

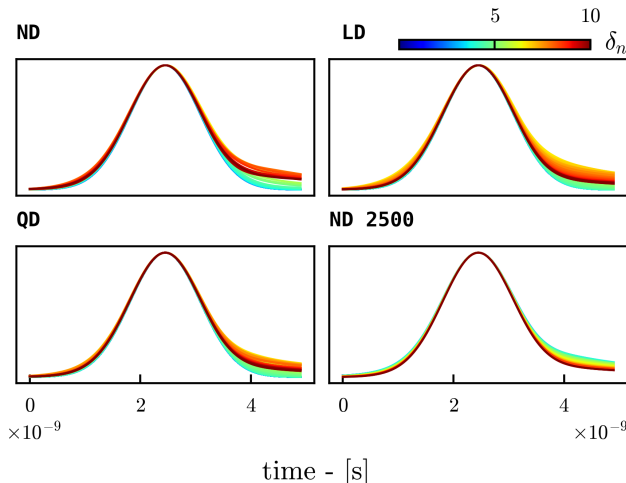


Figure 4.1: For all density profile, the pulse shape is getting broader and broader for large perturbations, and the delay is getting larger and larger. This is due to the presence of multiple scattering, and dispersive effects. This will be characterized further by the study of the mean skewness of the pulse shape.

One way to visualize that is plotting the distribution of some parameters of the pulse shape for different perturbation amplitude. Here we choose to study the rms and the amplitude of the pulse. Indeed, it allows to the behavior of the pulse width and height during the linear-non linear transition. This is shown in the following figure. This type of plots are called violins plot, where filled zone stands for the distribution of the random variable, calculate over every samples.

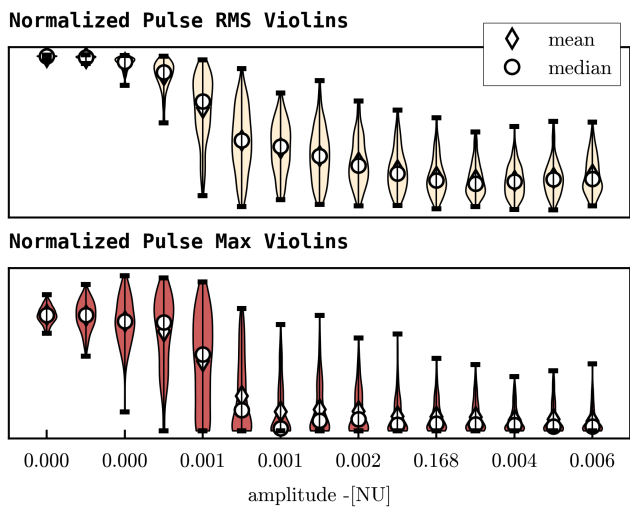


Figure 4.2: Here we plot the distribution of the pulse rms and amplitude for different perturbation amplitude, for the linear profile background profile **LD**. The distribution of the pulse rms and amplitude is getting broader and broader during the transition regime, this is due to randomness introduced by the perturbations, which seems to remain at large amplitudes, even if the distribution is getting quite constant. Let's also note that the mean of both distribution is getting smaller due to presence of multiple scattering, reaching a plateau at high turbulence amplitude.

The characteristic turbulence amplitude scale for the pulse shape transition seems to be the first critical value with $\delta n \approx 1e^{-3}$. Thanks to this study, we can unearth a way of characterizing the transition regime, using the pulse shape for multiple background profiles. For deeper insights about the pulse transition regime, we can study the skewness of the pulse shape, which should give us more information about the "broader and broader" distribution of the pulse shape. Note that we are talking about the transition regime of the pulse shape, since the transition regime regarding the delay seems to appear at much larger amplitude at the second critical value $\delta n \approx 1e^3$ as shown in Fig.2.3. One important question we have to solve is the following, which metrics is the most relevant to characterize the transition regime. This will help us, to build a relevant datasets to tackle the non linear regime.

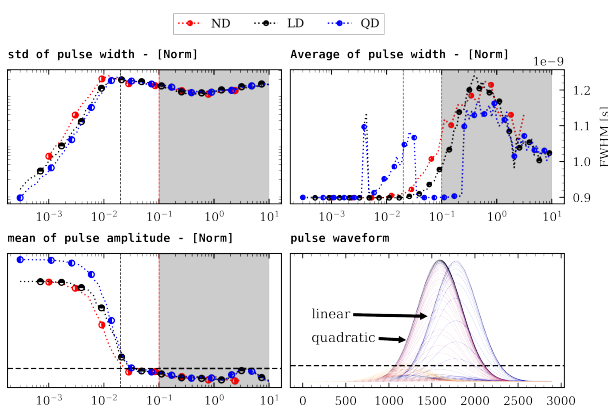


Figure 4.3: Here we plot three different metrics to characterize the pulse shape, the std of the pulse width, which is increasing (WHY), the average width is increasing as intended due to the superposition of multiple scattered pulse, for the mean pulse amplitude, it's decreasing for the same causes, however let's note that after the transition regime the mean pulse amplitude seems to increase again reaching a maximum at the amplitude value 5, the linearized turbulence turbulence density profile is also decayed from the simple linear background profile. This is easily understandable since we decrease the mean density turbulence amplitude in the plasma by linearizing the perturbation profile. One final thing to remark is the decay between the quadratic and the linear delays, indeed the quadratic profile has a little advance over the linear one. This is possibly due to the concave shape of the background quadratic profile. Indeed, thanks to the concavity, it's much easier to turbulence to reach the cut-off layer, and to perturb it.

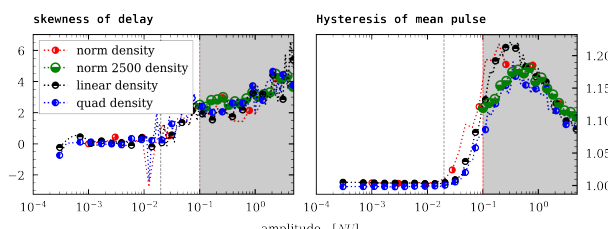


Figure 4.4: skewness of the delay shape, for different background profile, and perturbation amplitude. The skewness is getting larger and larger for large perturbations, this is due to the presence of multiple scattering, and dispersive effects. The hysteresis of the pulse is calculating using the ratio of the right area over the left area of the pulse, this allows to see the asymmetry of the pulse shape which is a measurement of the skewness of the pulse. The true Skewness of the pulse does not unearth smoothly the transition regime, this is why it is not tackled here.

2 Gaussian fitting of the pulse

On way to see the deformation of the gaussian pulse is to track the relative error of the gaussian pulse with a gaussian fit. Furthermore, it allows to study the true gaussian standard deviation, mean and amplitude. This is shown in the following figure, where we plot the relative error of the gaussian fit, and the gaussian fit

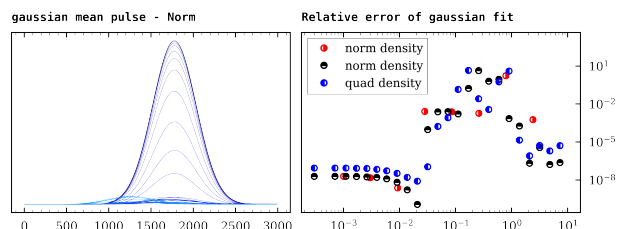


Figure 4.5: The relative error of the Gaussian fit (residuals ponderated by the size of the respective pulse amplitude) is getting large for the transition zone of the pulse shape, and seems to decline for very large turbulence. However we have to find smooth metrics to characterize the transition, and not a pseudo-random one to have better predictions in the next part. The gaussian parameters are also good quandidates and are plotted in the next figure

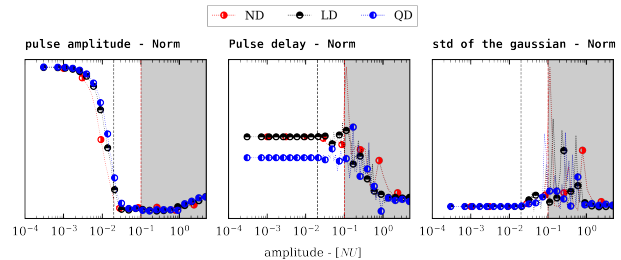


Figure 4.6: Gaussian pulse delay and standard deviation have chaotic behavior during the transition regime, this made them not relevant candidate for the next study. However lets note that the gaussian pulse amplitud, have quite a smooth behavior, but unearth a plateau during the non linear linear transition, which might not ne a good option, even if at large amplitude we capture the same behavior as for the non gaussian amplitude. In a much cleaner way, indeed it's clearly increasing, this might be interesting to study the highly non linear regime.

I Model collapses

As shown previously, the 1D model collapses for large perturbations. The goal of this chapter is to facilitate the deduction of the perturbations properties just from the typical study of the delayed pulse. Our goal will be to predict the perturbation amplitude, their typical correlation length and the original delay of the probing wave τ_0 without any perturbation. Using previous results, it might be quite simple to isolate the original delay and the turbulence amplitude, but the correlation length is a more difficult parameter to isolate, and seems to play a great role in the pulse properties. The non linear regime is a much more difficult regime to study, indeed the perturbations are large enough such that the cut-off layer is strongly perturbed, and the WKB approximation cannot be applied. The main goal of this approach is to find a way to link the plasma density perturbations to the reflected pulse delay. To retrieve some information about the pulse delay we will use a statistical approach to get rid of the randomness implies by the perturbations considerations.

II 1 dimensional study

To test the validity of the machine learning approach, let's try to tackle the non-linear regime using the 1D



dimensional approach. The 1D study didn't give the ability to retrieve information in this regime. To do so we will use the same approach as for the linear regime, but with a much larger perturbation amplitude. Different profiles will be used to see if the model succeeds in predicting the wanted features.

This exploration of the density profile is motivated by

Bibliography

¹T. J. Dolan, "Plasma heating and current drive", in *Magnetic fusion technology*, edited by T. J. Dolan (Springer London, London, 2013), pp. 175–232.

²A. Piel, *Plasma physics: an introduction to laboratory, space, and fusion plasmas*, Graduate Texts in Physics (Springer International Publishing, 2018).

³L. Qi, "Energy transfer of trapped electron turbulence in tokamak fusion plasmas", *Scientific reports* **12**, 5042 (2022).

⁴Y. Xiao and Z. Lin, "Turbulent transport of trapped-electron modes in collisionless plasmas", *Phys. Rev. Lett.* **103**, 085004 (2009).

⁵T. Xie, Y. Z. Zhang, S. M. Mahajan, F. Wu, H. He, and Z. Y. Liu, "The two-dimensional kinetic ballooning theory for trapped electron mode in tokamak", *Physics of Plasmas* **26**, 022503 (2019).

⁶W. Horton, "Drift waves and transport", *Rev. Mod. Phys.* **71**, 735–778 (1999).

⁷O. Krutkin, "Theoretical analysis and full-wave simulations combined in the development of the synthetic doppler reflectometry diagnostics for tokamaks", PhD thesis (June 2020).

⁸M. A. Mitsuru Kikuchi, *Frontiers in fusion research ii, introduction to modern tokamak physics*, edited by Springer (Springer, Naka, Ibaraki, Japan, Setagaya, Tokyo, Japan, 2015).

⁹K. Miyamoto, *Plasma physics and controlled nuclear fusion* (Jan. 2004).

¹⁰V. Rozhansky, *Plasma theory an advanced guide for graduate students* (Springer, St. Petersburg, Russia, 2023).

¹¹S. C. Prager, A. K. Sen, and T. C. Marshall, "Dissipative trapped-electron instability in cylindrical geometry", *Phys. Rev. Lett.* **33**, 692–695 (1974).

the fact that at the edge of the plasma, the relative amplitude of the turbulence profile is higher than in the core of the plasma. The simple linearization of the turbulence profile gives a constant envelope, whereas the non normalized one gives a divergent one at the edge. One solution was to introduce an exponential factor to the normalization.

¹²A. Hasegawa and M. Wakatani, "Self-organization of electrostatic turbulence in a cylindrical plasma", *Phys. Rev. Lett.* **59**, 1581–1584 (1987).

¹³M. Wakatani and A. Hasegawa, "A collisional drift wave description of plasma edge turbulence", *The Physics of Fluids* **27**, 611–618 (1984).

¹⁴B. Kadomtsev and O. Pogutse, "Trapped particles in toroidal magnetic systems", *Nuclear Fusion* **11**, 67 (1971).

¹⁵A. Hasegawa and K. Mima, "Pseudo-three-dimensional turbulence in magnetized nonuniform plasma", *The Physics of Fluids* **21**, 87–92 (1978).

¹⁶P. H. Diamond, *Theory of magnetically confined plasma*, <https://courses.physics.ucsd.edu/2021/Spring/physics218c/handouts.html>, 2021.

¹⁷Z. Lin, Y. Xiao, W. Deng, I. Holod, C. Kamath, S. Klasky, Z. Wang, and H. Zhang, "Size scaling and nondiffusive features of electron heat transport in multi-scale turbulence",

¹⁸G. Falchetto, J. Vaclavik, M. Maccio, S. Brunner, and L. Villard, "Applicability of the ballooning transform to trapped ion modes", *Physics of Plasmas* **7**, 1196 (2000).

¹⁹P. Aleynikov and N. B. Marushchenko, "3d full-wave computation of rf modes in magnetised plasmas", *Computer Physics Communications* **241**, 40–47 (2019).

²⁰O. Krutkin, S. Brunner, and S. Coda, "A method for density fluctuation measurements using pulse reflectometry", *Nuclear Fusion* **63**, 10.1088/1741-4326/acd5e0 (2023).

²¹J. R. Ruiz, F. I. Parra, V. H. Hall-Chen, N. Christen, M. Barnes, J. Candy, J. Garcia, C. Giroud, W. Guttenfelder, J. C. Hillesheim, C. Holland, N. T. Howard, Y. Ren, A. E. White, and J. contributors, "Interpreting radial correlation doppler reflectometry using gyrokinetic simulations", *Plasma Physics and Controlled Fusion* **64**, 055019 (2022).

REFERENCES

- ²²H. Biglari, P. H. Diamond, and P. W. Terry, “Influence of sheared poloidal rotation on edge turbulence”, *Physics of Fluids B: Plasma Physics* **2**, 1–4 (1990).
- ²³L. Vermare, P. Hennequin, Ö. D. Gürçan, C. Bourdelle, F. Clairet, X. Garbet, R. Sabot, and the Tore Supra Team, “Impact of collisionality on fluctuation characteristics of micro-turbulence”, *Physics of Plasmas* **18**, 012306 (2011).
- ²⁴J. W. Connor, R. J. Hastie, and J. B. Taylor, “Shear, periodicity, and plasma ballooning modes”, *Phys. Rev. Lett.* **40**, 396–399 (1978).
- ²⁵P. Molina Cabrera, S. Coda, L. Porte, A. Smolders, and T. Team, “V-band nanosecond-scale pulse reflectometer diagnostic in the tcv tokamak”, *Review of Scientific Instruments* **90**, 123501 (2019).